Order Parameter Modeling of Fluid Dynamics in Narrow Confinements Subjected to Hydrophobic Interactions

Suman Chakraborty*

Department of Mechanical Engineering, Indian Institute of Technology, Kharagpur- 721302, India

(Received 28 May 2007; published 31 August 2007)

A novel phase-field approach is developed for quantitative modeling of the complex thermophysics over reduced length scales in narrow fluidic confinements, as induced by the surface roughness-hydrophobicity coupling and the consequent hydrodynamic interactions. The method is tested for flows on micro- and nano- corrugated surfaces in narrow confinements, and the agreement with molecular dynamics and lattice Boltzmann simulations is found to be quantitative.

DOI: 10.1103/PhysRevLett.99.094504 PACS numbers: 47.61.−k

The physics of fluid-solid and fluid-fluid interactions in micro- and nanochannels has given rise to many complicated and unresolved apparent anomalies, primarily attributable to seemingly nontrivial dependences of the fluid flow characteristics on the molecular level interaction mechanisms and down-scaled topographical features of the confining boundaries. On system length scales, these details have often been abstracted with the notion of predefined sets of hydrodynamic boundary conditions, typically postulated on the basis of either ''no-slip'' or ''slip'' based conceptual paradigms [1–7], with an intention of mimicking the underlying molecular level interactions in an up-scaled continuum limit. However, the hydrodynamic interactions giving rise to these conjectures still remain to be poorly understood, especially within the purview of experimentally tractable spatiotemporal scales. This deficit stems from the complexities in describing the underlying thermofluidic interactions at physical scales that are substantially larger than those addressed in the pertinent molecular dynamics (MD) simulations.

Here what is proposed is believed to be the first complete phase-field description of fluid dynamics in narrow confinements subjected to hydrodynamic interactions originating out of complex hydrophobic effects [8]. A logical attempt is made to accommodate the implications of the disparate physical scales responsible for the underlying hydrodynamic interactions in a thermodynamically consistent manner. Significances of the present formalism lie in the fact that in a certain way, this provides an optimal compromise between the needs for embedding the underlying complex thermophysics through standard continuum based approaches that are unable to capture the disparate physical scales directly, and the needs for accessing computationally tractable as well as experimentally relevant physical scales that are truly beyond the reach of MD simulations. Notwithstanding their inherently mesoscopic character, the distribution of the effective chemical potential being introduced in this model is expected to represent no less physical content than its molecular-scale counterparts, reducing the requirements of an explicit capturing of the pertinent molecular transport features through expensive MD simulations that are otherwise intractable for most of the experimentally encountered physical scales.

Three distinctive and novel features are introduced into the present model to achieve the above-mentioned feat, in the context of micro- or nanoscale flows being subjected to hydrophobic interactions. First, a direct relationship is established between the effective contact angle and the surface order parameter variation, where the surface value of the order parameter automatically sets up the degree of ordering or disordering at the channel walls. Second, the features of hydrophobicity at small length scales are embedded in the order parameter description by introducing a modification in the chemical potential, which considers the rapidly-varying small length scale fluctuations about the slowly varying components of the order parameter and thereby implicitly accounts for the molecular-scale details of excluded volume regions over which the density varies rapidly. Third, the modifications of the local molecular fields due to the replacement of polar liquids by rigid walls are also taken into account, which are likely to trigger off separation-induced phase transition processes. With these physical considerations, it is established that the physics of hydrophobic interactions in microfluidic or nanofluidic confinements can be quantitatively reproduced by the generalized order parameter model, by comparing with recently reported MD simulations.

To emphasize the novel features of the present formalism, it may be instructive to briefly revisit a general phase-field framework, in which a liquid-vapor binary mixture can be characterized by means of a phase-field order parameter (effectively, a relative phase concentration distribution), $\phi = (n_1 - n_2)/(n_1 + n_2)$, where n_i are the number densities of the two species. The Ginzburg-Landau free energy for a binary mixture can be expressed in terms of a phase-field parameter as [9] $F(\phi) = \int[\frac{k}{2} \times (\nabla\phi)^2 + f(\phi)]d\vec{r} + \Psi_s$. The double-well potential contribution to $f(\phi)$ may be described as $\frac{B}{4}(\phi - \sqrt{\frac{A}{B}})^2(\phi + \sqrt{\frac{A}{B}})^2$, where $\phi_{\text{eq}} = \pm\sqrt{\frac{A}{B}}$ are two stable solutions of the equilibrium order parameter profile. The interfacial thickness, thus, is of the order of $\xi_{\text{int}} \sim \sqrt{\frac{k}{A}}$ (the mean-field correlation

length). The chemical potential, μ, can be defined as $\mu(\phi) = \frac{\delta F}{\delta \phi} = f'(\phi(\vec{r})) - k\nabla^2[\phi(\vec{r})]$. The equilibrium distribution of the order parameter [10], thus, can be obtained by setting $\mu(\phi) = 0$. The dynamic evolution of the order parameter is dictated by the Cahn-Hillard equation (advantages of this approach in analyzing the dynamical evolution of complex phase separating systems are detailed in [11]), which can be written as $\frac{\partial \phi}{\partial t} + \vec{v} \cdot \vec{\nabla}\phi = \vec{\nabla} \cdot (M\vec{\nabla}\mu)$, where M is the mobility of the order parameter. At the walls, the following zero-flux boundary conditions may be adopted: $\vec{n} \cdot \vec{\nabla}\phi = 0$, and $\vec{n} \cdot M\vec{\nabla}\mu = 0$, where $\vec{n}$ is a unit vector normal to the wall. The scales of the phase-field parameters that are related to the corresponding physical parameters are as follows: $B, A \sim k_B T_c$, and $\sqrt{kA} \sim \gamma_{\mathrm{lv}}$, where T_c is the critical temperature and γ_{lv} is the liquid-vapor surface energy. With the following choices of nondimensionalizing parameters: $t \rightarrow \frac{\xi_{\mathrm{int}}^2}{kAM}$, $\phi \rightarrow \sqrt{\frac{A}{B}}$, $l \rightarrow \frac{\sqrt{\xi_{\mathrm{int}}}}{k}$, $u \rightarrow l/t$, $\mu \rightarrow B\phi^3$, $p \rightarrow \frac{\eta AM\bar{k}}{\xi_{\mathrm{int}}^2}$, where $\bar{k} = \frac{k}{A\xi^2}$ (with $\xi_{\mathrm{int}} = \xi/\sqrt{\bar{k}}$), the nondimensional forms of the coupled Cann-Hilliard/Navier-Stokes equations (Model H [11]) become $\frac{\partial \phi}{\partial t} + \vec{v} \cdot \vec{\nabla}\phi = \nabla^2\mu$, and $(\frac{\partial \vec{u}}{\partial t} + \vec{u} \cdot \vec{\nabla}\vec{u}) = D_r[-\vec{\nabla}p + \vec{\nabla} \cdot (\nabla\vec{u} + \nabla\vec{u}^T) + C\mu\vec{\nabla}\phi]$, where $D_r = \frac{\eta}{\rho AM}$ is the ratio of the momentum diffusivity and the diffusivity of the order parameter, and $C = \frac{\gamma_{\mathrm{lv}}\xi}{\eta AM\sqrt{k}}$.

The above generic order parameter model description remains far from being complete, with regard to its inherent capability in capturing certain interesting aspects of fluid dynamic interactions in narrow confinements, typically attributed to the complicated and nontrivial hydrophobic interaction mechanisms. Despite an emerging consensus on some of the key features of such interactions, it has been hard to reconcile the fundamental modalities of interlinkage between the wettability conditions at the hydrodynamic scales, separation- and confinement-induced hydrodynamic interactions, and an apparently unpredictable nucleation of tiny vapor bubbles, from the perspective of conventional thermofluidic analysis. Notwithstanding the underlying details, however, the interfacial free energies of the phase transition point can be described as $\gamma_{\mathrm{sl}} = \Omega(\phi_s, -1) + \gamma_0$, $\gamma_{\mathrm{sv}} = \Omega(1, \phi_s) + \gamma_0$, $\gamma_{\mathrm{lv}} = \Omega(1, -1)$, where $\Omega(\phi_1, \phi_2) = \int_{\phi_1}^{\phi_2}[2k\nabla f(\phi)]^{0.5}$, and ϕ_s is the local surface value of the order parameter. Here the subscripts s, l, and v refer to substrate, liquid, and vapor, respectively, and ϕ is set in such a manner that $\phi = -1$ represents the liquid whereas $\phi = 1$ represents the vapor phase. From the above considerations, the contact angle at the wall can be written as a function of the corresponding order parameter as $\cos\theta_w = \frac{\gamma_{\mathrm{sl}} - \gamma_{\mathrm{sv}}}{\gamma_{\mathrm{lv}}} = \frac{3\phi_s - \phi_s^3}{2}$. The value of ϕ_s, thus explicitly sets up the degree of ordering or disordering at the -wall-fluid interface. Experimental perspectives of the contact angle determination for such small-scale systems are reported elsewhere [12].

The other parameters that are explicitly governed by the local surface wettability conditions are the short-ranged component of the wall-fluid interactions, which are confined within a length scale that is comparable to the order of ξ_{int}. Accordingly, the interfacial free energy at the substrate locations can be estimated by balancing the distortion energy with the fluid-solid interaction energy; the distortion energy being distributed over a layer with thickness of the same order of magnitude as that of the diffuse interface. Such short-range wall-fluid interactions can be represented by its corresponding surface potential as [9] $\Psi_s = \int[-h\phi_s - \frac{1}{2}g\phi_s^2]d\vec{r}$, where the parameters h and g are termed as the short-range surface field and the surface enhancement, respectively. The parameter h physically represents the preference of the substrate for either the liquid or the vapor and is related to the contact angle as [13] $\sqrt{\frac{2}{kB}}h = 2\,\mathrm{sgn}(\pi/2 - \theta_w)[\cos\frac{\alpha}{3}(1 - \cos\frac{\alpha}{3})]^{0.5}$, where $\alpha = \cos^{-1}(\sin\theta_w)$, and $\mathrm{sgn}(x) =$ sign of x. The parameter g represents the ''missing'' liquid-liquid interactions due to the fact that a near-wall liquid molecule has only a small number of liquid neighbors, and its exact quantification is detailed in [14]. The nucleation of nanobubble layers adhering to the hydrophobic surfaces represents the nonclassical case of ordering of vapor molecules abutting the wall, which represents the limiting case of ultra-short-range fluid-solid interaction over liquid-vapor interfacial length scales.

The above considerations for hydrophobic interactions, by no means, present a complete physical picture, since all interactions are not necessarily dictated by surface wettability constraints. To obtain a more complete picture, the contributions of excluded volume regions over which small-scale fluctuations in the density are expected to occur need to be aptly considered, which have so far not been taken into account in the literature of order parameter description for small-scale flows. As such, it is well known that hydrophobic units are not thermodynamically favored to form hydrogen bonds with water molecules. Hence, these give rise to excluded volume regions encompassing the locations characterized with rapidly diminishing number density of water molecules. Close to small hydrophobic units, water molecules can structurally change and reorganize without sacrificing their hydrogen bonds. However, close to larger hydrophobic units, persistence of a hydrogen bond network is virtually impossible. A drying effect [15], induced by the consequent energetic interactions, might lead to strong attraction between two hydrophobic surfaces. Further, loss of hydrogen bonds close to any such hydrophobic surface effectively repels liquid molecules, thereby favoring the formation of thin vapor layers. Such small-scale density fluctuations can be assumed to follow Gaussian statistics with a variance given as $\chi(\vec{r}, \vec{r}') = \langle \delta\phi(\vec{r})\delta\phi(\vec{r}') \rangle$. Hydrophobic interactions, in effect, exclude water from specified volumes, and the resultant solvation free energies are related to the probability of finding these volumes as empty in unperturbed fluids. This gives rise to an excess equivalent chemical potential, given as $\Delta\mu_{\mathrm{ex}} = -k_B T \ln[\frac{Z_v(0)}{\sum_{N \geq 0} Z_v(N)}]$, where $Z_v(N)$ is the

partition function for the case when N solvent molecules occupy the volume v, and is given by [16] $Z_v(N) = \exp\{-F(\phi(\vec{r}; N))/k_BT - [N - \int_v d\vec{r}\phi(\vec{r}; N)]^2/2\sigma_v - (\ln\sigma_v)/2\}$, and $\sigma_v = \int_v d\vec{r} \int_v d\vec{r}'\chi(\vec{r}, \vec{r}')$.

A third consequence of the small-scale hydrodynamic interactions, as mentioned earlier, is that in confined fluids, long-ranged interactions can also trigger separation-induced phase transitions. Such separation-induced cavitation physically originates from an increase in the local molecular field due to the replacement of polarizable fluids by solid walls. Physically, it is impossible for a hydrogen bond network to persist close to a hydrophobic surface. The underlying energetic effect may lead to drying, which can lead to strong attractions between the separated surfaces. For instance, the loss of hydrogen bonds near the hydrophobic surfaces effectively expels liquid water to move away, thereby forming thin vapor layers. Such interfacial fluctuations can destabilize the liquid further away from the solid walls, leading to a pressure imbalance. This effectively gives rise to an attractive potential between the two surfaces. The confinement effects, therefore, reduce the chemical potential by an amount $\Delta\mu_{\text{sep}}$, which, in the mean-field approximation [17], is given by $\Delta\mu_{\text{sep}} = \frac{2\pi\varepsilon\rho_l\sigma^3}{3}[(\frac{H}{2} + z)^{-3} + (\frac{H}{2} - z)^{-3}]$, where the confining walls of the channel are given by $z = 0$ and $z = H$, respectively. Here ε is the depth of the Lennard-Jones potential well and σ is the collision parameter.

The resultant chemical potential, $\mu_{\text{eff}} = \mu + \Delta\mu_{\text{ex}} - \Delta\mu_{\text{sep}}$, obtained as a combined consequence of all the effects mentioned as above, predicts the extent of hydrophobic interactions within the fluidic confinement, including the inception of nanobubbles that occurs when the driving force required to minimize the area of liquid-vapor interface is smaller than the forces that pin the contact line of the substrate. The consequent enhancement in concentrations of gas-filled submicrocavities close to the hydrophobic wall results in a deviation of the value of ϕ from its value at the bulk liquid phase, as captured by the present mathematical model. This, in turn, leads to a decrement in viscosity near the wall (note that a higher value of ϕ implies a lower value of effective viscosity). With the bulk phase viscosity still being employed for the continuum fluid flow calculations; this decrement in effective viscosity needs to be compensated with a consequent enhancement in the local shear strain rate, in order to achieve continuity in the shear stress (rate of momentum transport), giving rise to "apparent slip" effects.

In order to assess the predictive capability of the present model vis-à-vis the benchmark MD simulations [18], a rectangular groove of depth H_1 and width $H = L\text{-}a$ is considered to be introduced at the bottom wall of a nanochannel, as an artificially designed surface roughness element, as shown in the inset of Fig. 1. Periodic boundary conditions are considered with a periodicity of L. To render the present simulation studies comparable with the other reported studies [8,18], following simulation parameters

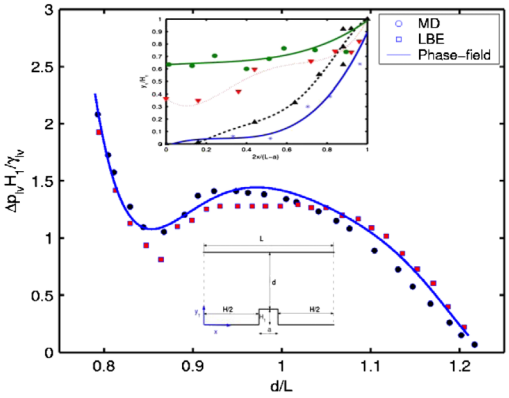

FIG. 1 (color online). Normalized pressure drop between the bulk phases, as a function of the normalized separation distance. The bottom inset schematically represents the problem geometry. In the top inset a few equilibrium interface profiles are shown. At high pressures, the liquid virtually occupies all spaces. Transition from this normal state tends to first occur at $d/l \approx 0.8$. The bottommost curve in the top inset marks that transition. The dashed line located above this curve is a subsequent snapshot of the interface at $d/l \approx 0.9$. The two curves at the top (corresponding to $d/l \approx 1$ and $d/l \approx 1.1$, respectively) represent partially dewetted states at lower pressures, leading to the formation of completely detached interfaces from the base of the substrate. Such transitions from normal to superhydrophobic states are also confirmed from the corresponding MD simulations [18]. The equilibrium interfacial locations depicted in the inset also compare well with the MD simulation predictions (shown by markers in the inset), even to a quantitative extent. The small-scale solvent fluctuations become significantly more important as the distance of separation "d" is progressively reduced, especially in the limit as $d/\sigma \to 1^-$. In the figure, LBE represents simulation results obtained by solving the lattice Boltzmann equations.

are considered: $H_1 = 10.7\sigma$, $L_1 = 18.9\sigma$, $L - a = 15.6\sigma$. The presence of the groove triggers the formation of a vapor film, at a critical pressure drop between the liquid and the vapor phase that is of the order of the capillary pressure (so that there is a reduction in Gibbs free energy on formation of a superhydrophobic state from the normal state), given by $p_{\text{cap}} = \frac{-2\gamma_{\text{lv}}\cos\theta_w}{L\text{-}a}$ (Here γ_{lv} is taken as 0.022 N/m, which is in the tune of $18k_BT$ [16], approximately corresponding to a temperature of 540 °C [8]). The other relevant parameters are taken as follows: $\frac{k_BT}{\varepsilon} = 1$ [17], $\frac{g}{k_BT} = -\frac{1}{6} + \frac{T_c - T}{T_c}$ [14], $\rho_l\sigma^3 = 0.75$ [17], $\frac{k}{k_BT} = B\xi^2$ where $B \approx 230$ kJ/cm^3/mol^2 and $\xi \sim 0.38$ nm [16]. The parameter A is estimated by noting that $\frac{\gamma_{\text{lv}}}{k_BT} \sim \sqrt{kA}$. The only fitting parameter, M, required for coupling the phase field with the flow field, is set with a consideration [19] that the Cahn number, C, is the ratio of the interfacial thickness (ξ) and the characteristic length scale of the surface perturbation or roughness element (H_1), based on which the value of M can be determined. The variation of the normalized pressure drop between the two bulk phases, as a function of d/L, is plotted in Fig. 1. It can be observed from Fig. 1 that the results from the MD

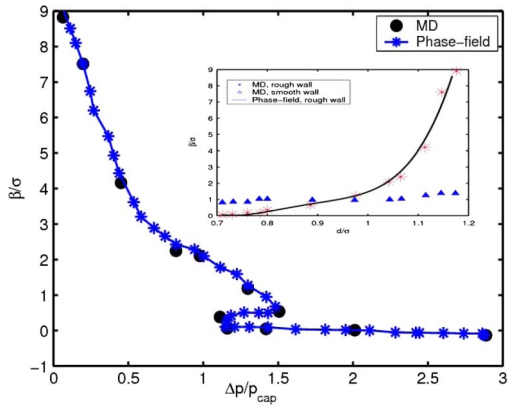

FIG. 2 (color online). Normalized slip length as a function of $\Delta p/p_{\mathrm{cap}}$. In the inset, the same is also depicted as a function of the normalized separation distance. The triangular markers represent slip length values for smooth walls (i.e., $H_1 \rightarrow 0$). The simulation results correspond to a shear-induced flow by moving the upper wall with a velocity U and the lower wall with a velocity $-U$. The slip length, β (independent of U with typically linear velocity profiles) is determined as the distance between the wall position (bottom layer of the substrate) and the depth at which the extrapolated velocity profile reaches the nominal wall velocity, U. The inset shows that in the normal state ($d/\sigma < 1$, approximately), the slip length is found to be rather small (roughness reduces slip), whereas in the superhydrophobic state the slip length is substantially enhanced.

simulation [18], Lattice Boltzmann simulation [8] and the present model are in excellent agreement, without necessitating any additional fitting parameters. The lattice Boltzmann model employed for this purpose is a minimal discrete version of the Boltzmann equation with external forcing terms being introduced to capture interparticle interactions and exponentially decaying forcing functions to mimic fluid-wall interactions [12]. In Fig. 1, the plateaus in the pressure drop characteristics over the range $0.9 < d/L < 1.1$ represent the pressure and density states at which the fluid invades the surface corrugation, thereby forming an interface that does not touch the bottom of the channel. With further reductions in d (implying increments in the average density) over the range $0.8 < d/L < 0.9$, however, the interface tends to touch the bottom wall, giving rise to an alteration in convexity of the characteristic curve.

The simulation results are finally expressed in terms of the variations in the normalized slip length (β), as a function of $\Delta p/p_{\mathrm{cap}}$, as shown in Fig. 2, corresponding to the situation of a parallel Couette flow. Following the trend apparent in the inset of Fig. 2, the β versus Δp characteristics depict a transition from normal to superhydrophobic behavior for $\beta/\sigma > 1$ (approximately). This physically implies that close to the wall one can observe a local phase transition that is triggered by the presence of the groove. This generic and spontaneous phenomenon leads to the formation of a gas layer in the vicinity, eventually resulting in the inception of a thermodynamic state in which gas and liquid phases can independently coexist. The incipient vapor layer formed on the solid surface and dynamically segregated from the liquid phase tends to augment the level of slippage. The vapor layer, in effect, acts like a shield, preventing the liquid from being directly exposed to the surface irregularities. In such cases, the liquid is not likely to feel the presence of the wall directly and may smoothly sail over the intervening vapor layers, instead of being in proximate contact with the wall roughness elements.

To summarize, a phase-field method is devised for quantitative modeling of hydrophobic interactions in narrow fluidic devices in the presence of small-scale geometrical irregularities. Such order parameter descriptions, in principle, can also be applied to the equilibrium theory of hydrophobic molecular solvation. While MD simulations would otherwise be ideal to study such systems, they are unfortunately unable to track most of the experimentally accessible spatiotemporal length scales. A further advantage of the present approach lies in the fact that the computational constraints are much less severe than the other equivalent methods, without necessitating the employment of several empirically fitted parameters.

*suman@mech.iitkgp.ernet.in

[1] E. Lauga and M. P. Brenner, Phys. Rev. E **70**, 026311 (2004).
[2] D. C. Tretheway and C. D. Meinhart, Phys. Fluids **16**, 1509 (2004).
[3] R. Benzi *et al.*, Europhys. Lett. **74**, 651 (2006).
[4] B. Li and D. Kwok, Phys. Rev. Lett. **90**, 124502 (2003).
[5] J. Harting *et al.*, Europhys. Lett. **75**, 328 (2006).
[6] J. W. G. Tyrrell and P. Attard, Phys. Rev. Lett. **87**, 176104 (2001).
[7] S. Granick *et al.*, Nat. Mater. **2** 221 (2003); S. Chakraborty, Appl. Phys. Lett. **90**, 034108 (2007).
[8] M. Sbragaglia *et al.*, Phys. Rev. Lett. **97**, 204503 (2006).
[9] D. Andrienko, B. Dünweg, and O. I. Vinogradova, J. Chem. Phys. **119**, 13 106 (2003).
[10] D. Jansnow and J. Vinals, Phys. Fluids **8**, 660 (1996).
[11] P. C. Hohenberg and B. I. Halerin, Rev. Mod. Phys. **49**, 435 (1977); V. E. Badalassi, H. D. Ceniceros, and S. Banerjee, J. Comput. Phys. **190**, 371 (2003).
[12] D. Ross, D. Bonn, and J. Meunier, J. Chem. Phys. **114**, 2784 (2001); T. R. Jensen *et al.*, Phys. Rev. Lett. **90**, 086101 (2003).
[13] A. J. Briant, P. Papatzacos, and J. M. Yeomans, Phil. Trans. R. Soc. A **360**, 485 (2002).
[14] D. Ross *et al.*, Phys. Rev. Lett. **87**, 176103 (2001).
[15] F. H. Stillinger, J. Solution Chem. **2**, 141 (1973).
[16] K. Lum, D. Chandler, and J. D. Weeks, J. Phys. Chem. B **103**, 4570 (1999).
[17] D. R. Berard, P. Attard, and G. N. Patey, J. Chem. Phys. **98**, 7236 (1993).
[18] C. Cottin-Bizonne *et al.*, Eur. Phys. J. E **15**, 427 (2004).
[19] X. Shan and H. Chen, Phys. Rev. E **47**, 1815 (1993); J. Zhang and D. Kwok, Phys. Rev. E **70**, 056701 (2004).